AIAA 2000-0900
Aerodynamic Characteristics, Database Development and Flight Simulation of the X-34 Vehicle

Bandu N.Pamadi,
Gregory J. Brauckmann
NASA Langley Research Center
Hampton, VA

Michael J. Ruth
Henri D. Fuhrmann
Orbital
Dulles, VA

38th Aerospace Sciences Meeting & Exhibit
10-13 January 2000 / Reno, NV

AERODYNAMIC CHARACTERISTICS, DATABASE DEVELOPMENT AND FLIGHT SIMULATION OF THE X-34 VEHICLE

Bandu N.Pamadi* and Gregory J. Brauckmann,†
NASA Langley Research Center, Hampton, VA 23681

Michael Ruth‡ and Henri Fuhrmann§
Orbital , Dulles, VA 20166

ABSTRACT

An overview of the aerodynamic characteristics, development of the preflight aerodynamic database and flight simulation of the NASA/Orbital X-34 vehicle is presented in this paper. To develop the aerodynamic database, wind tunnel tests from subsonic to hypersonic Mach numbers including ground effect tests at low subsonic speeds were conducted in various facilities at the NASA Langley Research Center. Where wind tunnel test data was not available, engineering level analysis is used to fill the gaps in the database. Using this aerodynamic data, simulations have been performed for typical design reference missions of the X-34 vehicle.

NOMENCLATURE

b	Wing span
C_i	Generalized aerodynamic coefficient
C_D	Drag coefficient
C_L	Lift coefficient
C_l	Rolling-moment coefficient
C_m	Pitching-moment coefficient
C_n	Yawing-moment coefficient
C_Y	Side-force coefficient
h	Height of the moment reference point above the ground plane, ft
M	Mach number
α	Angle of attack, deg
β	Angle of sideslip, deg
δ_a	Aileron deflection angle, deg
δ_e	Elevon deflection angle, deg
δ_{bf}	Body flap deflection angle, deg
δ_r	Rudder deflection angle, deg
δ_{sb}	Speedbrake deflection angle, deg
ΔC_i	Incremental in generalized aerodynamic coefficient C_i

INTRODUCTION

The X-34 vehicle being developed by the Orbital Sciences Corporation for National Aeronautics and Space Administration (NASA) is an integral part of the reusable launch vehicle (RLV) technology program currently being pursued by NASA with industry partnership. A schematic representation of the RLV technology demonstration path is shown in Figure 1. The primary goal of the RLV program [1] is to develop key technologies that will significantly lower the cost of access to space. The X-34 program originally started in spring of 1995 when the team of Orbital Sciences Corporation and Rockwell International was awarded a NASA contract to build an unmanned, fully reusable, two-stage, orbital vehicle capable of delivering approximately 1500 lb payload to

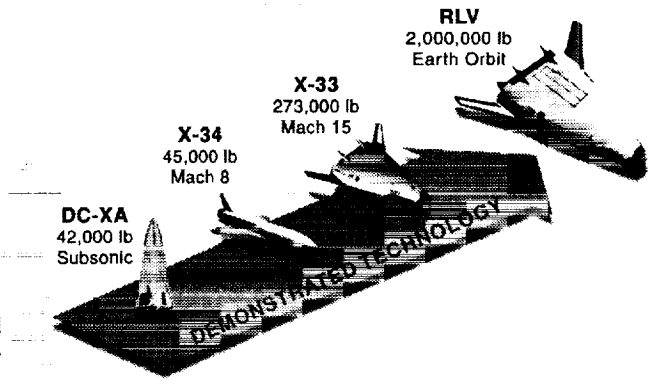

Figure 1. RLV technology demonstration path.

Aerospace Engineer, Vehicle Analysis Branch, Aerospace Systems Concepts and Analysis Competancy, Associate Fellow AIAA.
†*Aerospace Engineer, Aerothermodynamics Branch, Aerodynamics and Aerothermodynamics Competancy, Senior Member, AIAA.*
‡*Technical Manager for Guidance, Navigation and Control, Member AIAA.*
§*Aerospace Engineer, Aerodynamics, Member AIAA.*

low-earth orbit. However, the program was cancelled in late 1995 when Orbital Sciences Corporation and Rockwell determined that the program was not economically feasible. This program was resurrected in spring of 1996 when NASA solicited proposals on a different vehicle, also designated X-34 [2]. Orbital Sciences Corporation (now Orbital) was awarded this contract in June 1996.

The current X-34 vehicle is an unmanned suborbital, technology demonstrator vehicle capable of reaching an altitude of 250,000 ft and a speed of Mach 8. Some of the key technologies related to RLV that will be demonstrated by the X-34 vehicle include primary and secondary composite structures, advanced thermal protection systems (TPS), low cost avionics, rapid turn around times, autonomous flight including landing, and all weather airplane-like operations.

The NASA Langley Research Center (LaRC) is involved in the aerodynamic analysis, wind tunnel testing from subsonic to hypersonic speeds and the development of the preflight aerodynamic database of the X-34 vehicle. Orbital is responsible for the flight simulation of the X-34 vehicle. An analysis of the X-34 wind tunnel test data up to Mach 6 was reported in [3]. The formulation and development of the aerodynamic database was discussed in [4]. Since then, Mach 10 wind tunnel tests have been performed and with this, all the planned wind tunnel tests have been completed and the database has been updated. Orbital has performed numerous simulations for various design reference mission (DRM) trajectories that are expected to be flown during the X-34 flight test program. The objective of this paper is to present an overview of these activities and discuss salient aerodynamic and flight characteristics of the X-34 vehicle.

VEHICLE/MISSION DESCRIPTION

The X-34 vehicle has a close similarity with the Space Shuttle Orbiter but is relatively smaller in size. A schematic three-view diagram of the X-34 vehicle is presented in Figure 2. The X-34 vehicle has an overall length of about 58 ft, wing span of 28 ft and a height of about 12 ft. The approximate gross weight of the X-34 vehicle is 45000 lb. The main wing of the X-34 vehicle has a leading edge sweepback of 45°, a dihedral of 6°, and an 80° leading edge strake and full span split elevons (from actuator torque considerations). The elevons on the same side are always deflected together. Deflected symmetrically, elevons produce pitch control and asymmetric deflections provide roll control. The vehicle has a body flap located at the trailing edge of the fuselage. The body flap helps to shield the engine nozzle from aerodynamic heating at hypersonic speeds and also augments pitch control. The vehicle features a centerline, all movable vertical tail for directional stability/control. The vehicle also features reaction control system (RCS) jets located at the aft end of the fuselage for roll and yaw control when the vertical tail becomes ineffective at high altitude and high Mach number (low dynamic pressure and high angles of attack) flight conditions. The vertical tail has a split speedbrake like the Space Shuttle Orbiter for energy management during descent. The TPS system on X-34 consists of a mix of ceramic tiles and blankets. Ceramic tiles are used in the stagnation regions of the nose and wing leading edges where the aerodynamic

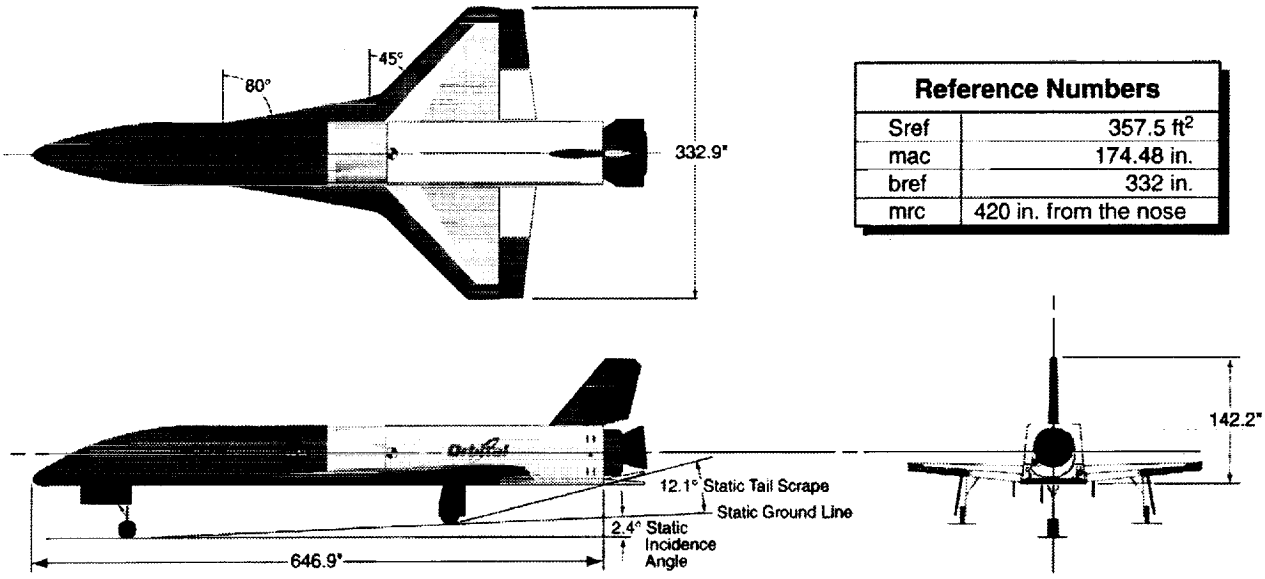

Figure 2. Schematic diagram of the X-34 vehicle.

heating is quite severe. Three types of blankets are employed for the rest of the acreage of the vehicle depending on the anticipated thermal environment. Additional information on the TPS can be found in [5].

The X-34 will be powered by the "Fastrac" rocket engine which is under development at the NASA Marshall Space Flight Center (MSFC), Huntsville, Alabama. The bi-propellent (liquid oxygen (LOX) and RP (kerosene)) Fastrac engine is designed for a nominal thrust of 60,000 lb and is expected to have a thrust vectoring capability of ±15° in the pitch plane. The X-34 vehicle has one composite RP tank and two aluminum LOX tanks located axially one behind the other. The RP tank is located in the front part of the fuselage and ahead of the two LOX tanks.

A typical X-34 mission profile is depicted in Figure 3. The X-34 vehicle will be "captive" carried under the belly of the L-1011 aircraft up to an altitude of about 38,000 ft and a Mach number of 0.7 at which point it will be released. The vehicle will be unpowered and all its control surfaces will be locked for about one second following the drop. Once the vehicle makes a safe separation from the L-1011 aircraft, the Fastrac engine will ignite and accelerate the vehicle towards its target altitude of 250,000 ft and target speed of Mach 8. After engine burn out, the vehicle will coast and glide back to earth and execute an autonomous, airplane-type landing on a conventional runway.

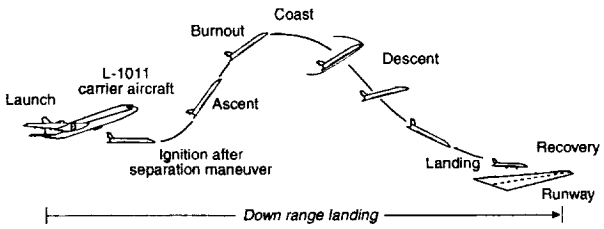

Figure 3. Typical X-34 flight profile.

FLIGHT TEST PROGRAM

The X-34 flight test program includes L-1011 captive carry testing, runway tow testing, unpowered approach and landing tests, and incremental powered envelope expansion flights up to the full Mach 8 capability. The captive carry tests serve to validate and provide FAA (Federal Aviation Administration) certification of the L-1011 as the carrier vehicle for the X-34. These tests were conducted at the NASA Dryden Flight Research Center (DFRC), California in the fall of 1999 up to the maximum captive carry flight Mach number of 0.87.

Early in 2000, the X-34 vehicle will undergo runway tow testing at the DFRC. These tests will be used to prove out the autonomous landing, steering, and braking algorithms. The unpowered X-34 vehicle will be towed up to a speed of about 80 mph with a truck and released. Tracking of the runway centerline, steering and braking effectiveness will all be monitored during the runway tow test. Following successful completion of the runway tow test, some additional L-1011/X-34 captive carry flights and "dry run" releases will be performed to prepare for the first approach and landing test in the spring of 2000. These approach and landing tests will be conducted at the White Sands Space Harbor in New Mexico and will validate the release, approach, landing, and rollout phases of the X-34 flight profile.

The Fastrac engine static fire testing will be conducted at the DFRC during the spring of 2000 and will be followed by low Mach powered flight of the X-34 vehicle in the summer of 2000. Subsequently, several flights will be conducted to gradually expand the flight envelope of the X-34 vehicle. It is proposed to collect aerodynamic data in these tests and use it to update the X-34 aerodynamics database for subsequent flights. Emphasis will be placed on envelope expansion, not operability, at this point in the program. The flight testing of the X-34 vehicle will then move to NASA Kennedy Space Center (KSC), Florida which will serve as the proving ground for X-34 operability. The X-34 vehicle will perform high Mach number flights off the Eastern coast from North Carolina down to the KSC. Flights will be conducted every two weeks for a three month proving period with minimal ground crew. A surge capability will also be demonstrated in which the vehicle will be turned around and flown within 24 hours which is an important requirement of the X-34 program.

The X-34 program is currently planning for 27 flights. These flights include experiments to demonstrate new technologies in TPS, structures, and composite liquid oxygen tanks. Additional flight experiments may include thermal and pressure measurements for validation of computational fluid dynamics and computational aerodynamic heating codes.

WIND TUNNEL TEST FACILITIES

A brief description of various LaRC wind tunnel facilities used in generating the test data included in the X-34 aerodynamic database is presented below. Additional information on these LaRC test facilities may be found in [6,7,8,9]. The L-1011/X-34 captive carry and separation aerodynamic model tests were conducted by

Orbital in the Calspan transonic wind tunnel facility. Also, some tests on the X-34 model were conducted in the trisonic wind tunnel facility at MSFC. These test results are not discussed in this paper.

LaRC 14- by 22-Foot Subsonic Tunnel

The Langley 14- by 22-Foot Subsonic Tunnel is a closed circuit, single return, atmospheric tunnel with a maximum speed of 338 ft/sec. The test section measures 14.5- by 21.8 ft and has a length of about 50 ft. The maximum unit Reynolds number is 2.1×10^6 per ft. The tunnel is equipped with boundary layer suction on the floor at the entrance to the test section.

LaRC 16-Foot Transonic Tunnel

The Langley 16-Foot Transonic Tunnel is a closed circuit, single return, continuous flow atmospheric tunnel. The test medium is air. This tunnel has a slotted wall, octagonal test section which measures 15.5 ft across the flats. The normal test Mach number ranges from 0.3 to 1.3. The angle of attack can be varied up to 25°. The unit Reynolds number varies from 2.0 to 4×10^6 per ft.

LaRC Unitary Plan Wind Tunnel

The Langley Unitary Plan Wind Tunnel (UPWT) is a continuous flow, variable pressure, closed circuit pressure tunnel having two separate test sections, called low Mach number test section (leg 1) and high Mach number test section (leg 2). Each test section measures 4- by 4 ft and has a length of 7 ft. The tunnel is capable of operating from near vacuum conditions to a pressure of 10 atmospheres. The low Mach number test section covers the Mach number range from 1.46 to 2.86 and the high Mach number test section from 2.3 to 4.6. The angle of attack capability is from −12° to 22° with possibility for testing at higher values using dogleg strings. The unit Reynolds numbers range from 1.0 to 4.0×10^6.

LaRC 20-Inch Mach 6 Tunnel

The Langley 20-Inch Mach 6 Tunnel is a blow down test facility that uses heated, dried and filtered air as the test medium. The test section measures 20.5- by 20-inches. Typical operating stagnation pressures range from 30 to 500 psi and the stagnation temperature from 750° to 1000° R. The unit Reynolds numbers range from 0.5 to 8×10^6 per ft. This tunnel has a capability to run continuously up to 15 minutes. The tunnel is equipped with a model injection system on the bottom of the test section that can insert a sheltered model into the air stream in less than 0.5 seconds.

LaRC 31-Inch Mach 10 Tunnel

The Langley 31-Inch Mach 10 Tunnel is a hypersonic blow down facility that uses dried, heated, and filtered air as the test gas. The facility typically operates at stagnation pressures from 350 to 1450 psia and at a stagnation temperature of 1850°R, with corresponding free stream unit Reynolds numbers of 0.5 to 2.2×10^6 per ft. A three-dimensional, contoured nozzle is used to provide a nominal freestream Mach number of 10 in the 31-Inch square test section. A side-mounted model injection system can insert models from a sheltered position to the tunnel centerline in less than 0.6 sec. Run times up to 3 minutes are possible with this facility although current test run times were on the order of one minute.

MODELS, INSTRUMENTATION AND TEST PROCEDURE

The model for the 14-ft by 22-ft low subsonic, free stream and ground effect tests was a 10% scale model of the X-34 outer mold line (OML) geometry inclusive of TPS. The test model had remote activation of elevons, body flap and rudder. The floor boundary layer suction was used in the X-34 ground effect tests. The ground effect test data was obtained for various separation heights (measured from moment reference point to the ground plane) ranging from 0.3 to 2.5 times wing span. The X-34 vehicle has two doors for the main gear, one on each side, but a single door for the nose gear, only on the left side. Therefore, when the nose gear is down and its door is open, the configuration becomes aerodynamically asymmetric giving rise to side force, rolling and yawing moments at zero sideslip.

The model for the 16-Foot Transonic Tunnel and the UPWT was a 0.033-scale model of the X-34 OML geometry, for the 20-Inch Mach 6 Tunnel was a 0.018 scale model of the X-34 OML geometry and that for the 31-Inch Mach 10 Tunnel was a 0.013-scale model of the X-34 OML geometry.

For the test models in the 14-by 22-Foot Subsonic Tunnel, the 16-Foot Transonic Tunnel and the UPWT (leg 1) tests, boundary layer transition trips were applied at the nose and the leading edges of the wing and vertical tail to promote turbulent flow over the test models. The models tested in the UPWT (leg 2), the 20-Inch Mach 6 Tunnel and the 31-Inch Mach 10 Tunnel were not tripped. However, the data from the UPWT (Leg 1) tests, where models with and without the trips were tested, showed that tripping had little effect on lift and pitching moment coefficients but resulted in a drag coefficient increase of about 2% for Mach 1.6 to 2.5.

The aerodynamic forces and moments were measured using six component strain gage balances. The balances used in the 20-Inch Mach 6 Tunnel and 31-Inch Mach 10 Tunnel were water cooled to minimize the balance temperature variations due to aerodynamic heating. Corrections were applied to the balance measurements to account for the temperature effects only for the 31-Inch Mach 10 Tunnel test data.

The force and moment data were acquired in a "pitch and pause" manner. The balance moment reference center, expressed in terms of full scale vehicle, was located at 420 inches from the nose. The base and cavity pressures were measured on all models except the model in the 31-Inch Mach 10 tests and these were used to make correction to the measured axial force. In the Mach 10 tests, owing to limitations of the model and cavity size, the cavity pressure could not be measured and no correction to the axial force was made.

In general, the tests in all the above facilities covered elevon deflections from –30° to +20°, aileron deflections of –30° to +20° (elevons on one side deflected, those on the other side held at zero), body flap deflections of –15° to +20°, rudder deflection of 5° to 30° and nominal speedbrake deflections of 30° to 90°. For subsonic and low supersonic tests (up to Mach 2.5), the angle of attack varied from –4° to 20°. For UPWT (leg 2) and Mach 6 tests, the angle of attack reached up to 36°. However, for Mach 10 tests, the maximum angle of attack ranged only up to 28°. The sideslip was in the range of –6° to +6° for tests in the 14-by 22-Foot Subsonic Tunnel, the 16-Foot Transonic Tunnel and the UPWT. For Mach 6 tests, the sideslip was in the range –3° to +4°. In all the tests up to Mach 6, the lateral/directional test data was obtained for angle of attack fixed with sideslip variations as well as sideslip fixed with angle of attack variations. However, for the Mach 10 tests, the lateral/directional test data was obtained with sideslip fixed at –3° and +3° and angle of attack varying from 0 to 28°.

The uncertainties in the balance measurements for various Mach numbers were estimated as follows: normal force from 0.001 to 0.0216, axial force from 0.0008 to 0.0054, pitching moment coefficient from 0.004 to 0.0177, side force coefficient from 0.0028 to 0.0179, rolling moment coefficient from 0.0005 to 0.0011 and the yawing moment coefficient from 0.0008 to 0.004. Additional information on the measurement uncertainties can be found in [3].

FORMULATION OF AERODYNAMIC DATABASE

An important aspect of developing the aerodynamic database is the formulation of suitable aerodynamic models. The development of aerodynamic models for the evaluation of the static aerodynamic forces and moments of the X-34 vehicle in free flight and for flight in ground effect is discussed in the following. This discussion does not include the control surface hinge moments and the dynamic or damping derivatives. This formulation is similar to that used in the Space Shuttle Orbiter data book [10].

Aerodynamic Coefficients in Free Flight

By free flight, it is meant that the vehicle is out of ground effect. This assumption generally holds when the vehicle is at a height exceeding 2.5 wing spans.

Assume that the vehicle is operating at a combined angle of attack and sideslip. Let C_i represent any one of the six aerodynamic coefficients C_L, C_D, C_m, C_Y, C_l or C_n and be given by

$$C_{i,total} = C_{i,b}(\alpha, M) + \Delta C_{i,\delta_e} + \Delta C_{i,\delta_a} + \Delta C_{i,\delta_{bf}} + \Delta C_{i,\delta_r} + \Delta C_{i,\delta_{sb}} + \Delta C_{i,LG} + \Delta C_{i,b,\beta} + \Delta C_{i,\delta_r,\beta} + \Delta C_{i,\delta_{sb},\beta} + \Delta C_{i,LG,\beta} \quad (1)$$

Here, $C_{i,total}$ is the total coefficient of the vehicle and is expressed as a sum of its value for the baseline at angle of attack (zero sideslip) $C_{i,b}(\alpha, M)$, and various incremental coefficients due to deflection of control surfaces like elevons (δ_e), ailerons (δ_a), body flap (δ_{bf}), rudder (δ_r), speedbrake (δ_{sb}) or the extension of landing gear (LG), all in zero sideslip ($\beta = 0$) plus the incremental coefficients due to sideslip for the baseline, deflection of rudder, speedbrake, and extension of the landing gear in the presence of sideslip. It is assumed that the sideslip has effect only on the baseline, and when the rudder and speedbrake are deflected but has no effect when elevons, body flap or ailerons are deflected.

The parameter $\Delta C_{i,\delta_e}$ denotes the incremental coefficient due to a elevon deflection and is defined as

$$\Delta C_{i,\delta_e} = C_i(\alpha, M, \delta_e) - C_{i,b}(\alpha, M) \quad (2)$$

The other incremental coefficients due to the deflection of body flap ($\Delta C_{i,\delta_{bf}}$), rudder ($\Delta C_{i,\delta_r}$), speedbrake ($\Delta C_{i,\delta_{sb}}$) and landing gear ($\Delta C_{i,LG}$) are defined in an identical manner as in equation (2). The parameter $\Delta C_{i,\delta_a}$ represents the incremental coefficient due to aileron deflections and is defined in a slightly different manner. For lift, drag and pitching moment coefficients

$$\Delta C_{i,\delta_a} = 0.5(\Delta C_{i,\delta_e=\delta_{e,L}} + \Delta C_{i,\delta_e=\delta_{e,R}}) - \Delta C_{i,\delta_e} \qquad (3)$$

Thus, to evaluate $\Delta C_{i,\delta_a}$, the elevon aero data is used twice, once assuming $\delta_e = \delta_{e,L}$ to obtain $\Delta C_{i,\delta_e=\delta_{e,L}}$ and then assuming $\delta_e = \delta_{e,R}$ to determine $\Delta C_{i,\delta_e=\delta_{e,R}}$. As a check, when aileron deflection is zero, i.e., $\delta_{e,L} = \delta_{e,R}$, $\Delta C_{i,\delta_a} = 0$ as expected.

The incremental coefficients due to sideslip are evaluated as follows:

For the baseline in sideslip, the incremental coefficient is defined as

$$\Delta C_{i,b,\beta} = C_i(\alpha, M, \beta) - C_i(\alpha, M) \qquad (4)$$

The incremental coefficient due to the deflection of rudder when the vehicle is in sideslip is defined as,

$$\Delta C_{i,\delta_r,\beta} = [C_i(\alpha, M, \beta, \delta_r) - C_i(\alpha, M, \beta)] - \Delta C_{i,\delta_r} \qquad (5)$$

The incremental coefficients due to speedbrake deflection or the extension of the landing gear are defined in an identical manner as in equation (5).

The formulation as given by equation (1) is of general nature. Usually, some of the incremental coefficients are zero. For example, $\Delta C_{y,\delta_e} = \Delta C_{y,\delta_{bf}} = \Delta C_{y,\delta_{sb}} = 0$. Additional details on the formulation of the free flight aerodynamic database may be found in [4].

Aerodynamic Coefficients in Ground Effect

Consider the vehicle with its landing gear fully extended and operating in the proximity of the ground (h/b ≤ 2.5). Here, h is the height of the vehicle above the ground plane, assumed equal to the vertical distance between the moment reference point and the ground plane, and b is the wing span. Let

$$C_i(\alpha, \beta, \delta_e, \delta_{bf}, \delta_{sb}, \delta_a, \delta_r, h/b) = C_i(\alpha, h/b = \infty) + \Delta C_i(\alpha, \beta, \delta_e, \delta_{bf}, \delta_{sb}, \delta_a, \delta_r, h/b) \qquad (6)$$

Here, it is assumed that the aerodynamic coefficient in ground effect is expressed as a sum of its value in free flight ($h/b = \infty$) for the baseline at angle of attack (zero sideslip) and an incremental coefficient due to the deflection of the control surfaces and ground effect. The inclusion of the term h/b in the parenthesis denotes that the coefficient C_i is evaluated in ground effect. As before, C_i denotes any one of the six aerodynamic coefficients C_L, C_D, C_m, C_Y, C_l or C_n. Assume that the incremental coefficient in equation (6) is given by

$$\begin{aligned}\Delta C_i(\alpha, \beta, \delta_e, \delta_{bf}, \delta_{sb}, \delta_a, \delta_r, h/b) = {} & \Delta C_i(\alpha, h/b) \\ & + \Delta C_i(\alpha, \delta_e, h/b) + \Delta C_i(\alpha, \delta_{bf}, h/b) \\ & + \Delta C_i(\alpha, \delta_{sb}, h/b) + \Delta C_i(\alpha, \delta_a, h/b) \\ & + \Delta C_i(\alpha, \delta_r, h/b) + \Delta C_i(\alpha, \beta, h/b) \\ & + \Delta C_i(\alpha, \beta, \delta_{sb}, h/b) + \Delta C_i(\alpha, \beta, \delta_r, h/b) \qquad (7)\end{aligned}$$

Here, $\Delta C_i(\alpha, h/b)$ represents the incremental coefficient for the baseline at angle of attack and in the presence of the ground with respect to the baseline in free flight at the same angle of attack and is defined as

$$\Delta C_i(\alpha, h/b) = C_i(\alpha, h/b) - C_i(\alpha, h/b = \infty) \qquad (8)$$

The parameter $\Delta C_i(\alpha, \delta_e, h/b)$ represents the incremental coefficient due to elevon deflection at angle of attack and zero sideslip and in the presence of the ground with respect to the baseline in zero sideslip at the same values of α, h/b and is defined as,

$$\Delta C_i(\alpha, \delta_e, h/b) = C_i(\alpha, \delta_e, h/b) - C_i(\alpha, h/b) \qquad (9)$$

The incremental coefficients due to the deflection of body flap, speedbrake, ailerons and rudder are defined in an identical manner as given in equation (9). Next, consider the incremental coefficients involving sideslip. The incremental coefficients due to sideslip are defined as,

$$\Delta C_i(\alpha, \beta, h/b) = C_i(\alpha, \beta, h/b) - C_i(\alpha, h/b) \qquad (10)$$

$$\Delta C_i(\alpha, \beta, \delta_r, h/b) = [C_i(\alpha, \beta, \delta_r, h/b) - C_i(\alpha, \beta, h/b)] - \Delta C_i(\alpha, \delta_r, h/b) \qquad (11)$$

$$\Delta C_i(\alpha, \beta, \delta_{sb}, h/b) = [C_i(\alpha, \beta, \delta_{sb}, h/b) - C_i(\alpha, \beta, h/b)] - \Delta C_i(\alpha, \delta_{sb}, h/b) \qquad (12)$$

Additional details on the formulation of ground effect aerodynamic model may be found in [4].

Process of Development of the Aerodynamic Database

The current X-34 program started in the summer of 1996. At that time, some preliminary wind tunnel test data at Mach 0.2 and at Mach 6 were available for the previous (cancelled) X-34 configuration. While the wind tunnel test program on the new X-34 configuration was yet to start, it was necessary to quickly put together an aero database for the guidance, navigation and control engineers to get started with the flight control system design. For this purpose, the first version of the aero database was developed using APAS (Aerodynamic Preliminary Analysis System) which is an interactive computer code capable of giving quick engineering estimates from subsonic to hypersonic speeds [11,12]. The APAS predictions were adjusted using the available wind tunnel data at Mach 0.2 and 6.0 for the previous version of the X-34. For other Mach numbers, past experience with similar vehicles such as the Space Shuttle Orbiter and other wing-body configurations was used to anchor the APAS predictions [13,14,15].

Subsequently, the aero database was regularly updated by replacing the APAS results with the wind tunnel test data as and when such data on the current X-34 model became available. All the planned wind tunnel tests were completed and the final update to the aerodynamic database was accomplished in October 1999.

As said before, the lateral/directional data from the 31-Inch Mach 10 tests were obtained only for sideslip of –3° and +3°. In view of this, several gaps exist in the Mach 10 test data. To fill these gaps and populate the database at Mach 10, APAS was used. The approach taken was to run APAS for Mach 6 and Mach 10, calculate the incremental coefficient due to Mach number variation from 6 to 10 when all other parameters remain constant. Next, add this incremental to the Mach 6 test data so that the Mach 6 test data is made applicable for Mach 10. As an example, consider the aerodynamic coefficient for the baseline vehicle at combined angles of attack and sideslip,

$$C_i(\alpha, \beta, M10) = C_i(\alpha, \beta, M6, WT) + \Delta C_i(APAS) \quad (13)$$

where

$$\Delta C_i(APAS) = C_i(\alpha, \beta, M10, APAS) - C_i(\alpha, \beta, M6, APAS) \quad (14)$$

The aerodynamic data in the aero database is presented in the form of tables so that the user can evaluate each of the terms appearing in the free flight and ground effect aerodynamic models. For the free flight aero database, the Mach number ranges from 0.3 to 10.0 with closely spaced values in the transonic regime. The angle of attack varies from –6° to 21° for M = 0.3 to 2.5 and from –5° to 40° for M = 3.0 to 10.0. The data is presented for elevon deflections (positive downwards) of –30° to 20°, aileron deflections from –30° to +20° (left elevons deflected, right held at zero), body flap deflections of –15° to 20°, rudder deflections (positive to left) from –5° to –20° and nominal speedbrake deflections from 30° to 90°. The sideslip ranges from –4° to +5°.The ground effect aerodynamic data is presented for Mach 0.3 and *h/b* varying from 0 to 2.5. The control deflections considered in the ground effect aerodynamic database are similar to those in the free flight aero database. All the aerodynamic data in the database is with respect to the moment reference point located at 420 inches from the nose.

RESULTS AND DISCUSSION

Aerodynamic Characteristics

Some of the salient aerodynamic characteristics of the X-34 vehicle are discussed in this section. For more details reference may be made to [3,4].

The variation of lift coefficient and pitching moment coefficient with angle of attack at various Mach numbers are presented in Figures 4 and 5. It is observed that the vehicle does not encounter stall up to 21° angle of attack in subsonic/supersonic range and up to 40° at hypersonic speeds. The vehicle is unstable at low speeds (M = 0.3) in pitch at low α, exhibits a pitch up tendency around α = 9° and then a stable break with further increase in α. The vehicle becomes more stable at tran-

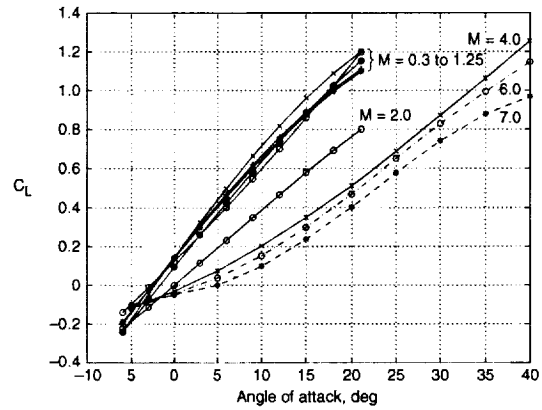

Figure 4. Variation of lift coefficient with angle of attack for various Mach numbers.

sonic/supersonic speeds and the angle of attack at which pitch up occurs also increases as observed in Figure 5. At hypersonic speeds, the vehicle becomes unstable because of the increasing lift developed by the forward parts of the fuselage and exhibits a tendency for a stable break at high angles of attack. This type of variation in pitching moment coefficient is typical of wing-body configurations at hypersonic speeds.

The variation of untrimmed lift-to-drag ratio is presented in Figure 6. It is observed that at low subsonic speeds, the vehicle has a lift-to-drag ratio of as much as 8 at low angles of attack. However, as Mach number increases the value of lift-to-drag ratio decreases and assumes values ranging from 1 to 2.

An example of elevon effectiveness from subsonic to hypersonic speeds is shown in Figure 7 for two values of angles of attack, $\alpha = 6°$ and 20°. For $\alpha = 6°$, it is observed that the elevon effect decreases rapidly at supersonic and hypersonic speeds. It is interesting to note that for $\alpha = 20°$, the downward deflected elevons still retain their effectiveness all the way up to Mach 10.

The variation of body flap effectiveness for $\alpha = 6°$ and 20° is shown in Figure 8. The data for the body flap deflection of −15° goes only up to Mach 4.6. As observed above for elevons, the body flap effectiveness decreases at supersonic/hypersonic speeds for $\alpha = 6°$ and for $\alpha = 20°$, the downward deflected body flap retains effectiveness all the way up to Mach 10.

Typical aileron effectiveness as measured by the rolling moment coefficient is shown in Figure 9 for $\alpha = 6°$ and 20°. It is observed that for $\alpha = 6°$, the aileron effectiveness decreases at supersonic and hypersonic speeds and for $\alpha = 20$, the downward deflected ailerons retain their effectiveness all the way up to Mach 10.

The rudder effectiveness as measured by the yawing moment coefficient is shown in Figure 10 for $\alpha = 6°$ and 20°. It is observed that the rudder effectiveness in-

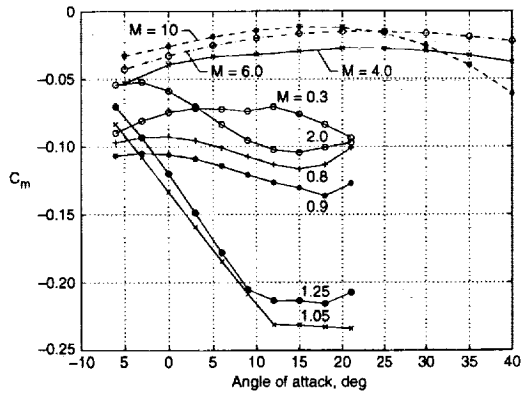

Figure 5. Variation of pitching moment coefficient with angle of attack for various Mach numbers.

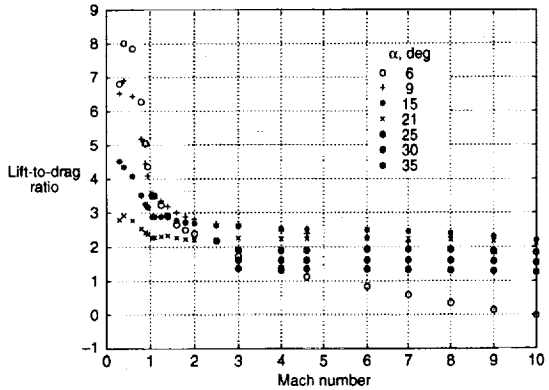

Figure 6. Variation of lift-to-drag ratio (untrimmed) with Mach number for various angles of attack .

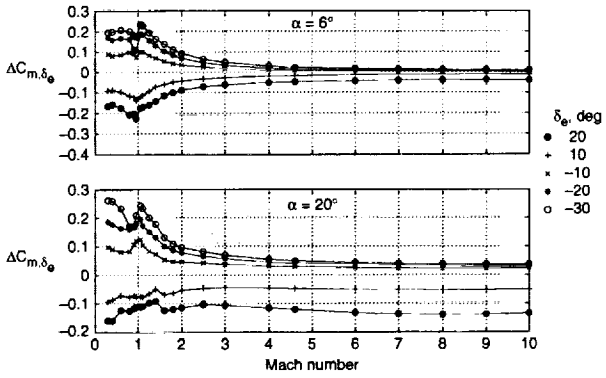

Figure 7. Elevon effectiveness at $\alpha = 6°$ and $\alpha = 20°$.

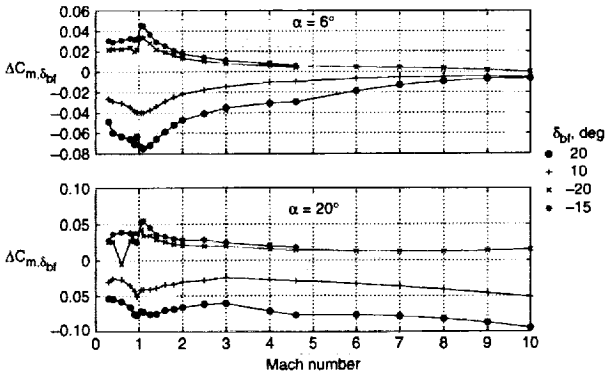

Figure 8. Body flap effectiveness at $\alpha = 6°$ and $\alpha = 20°$.

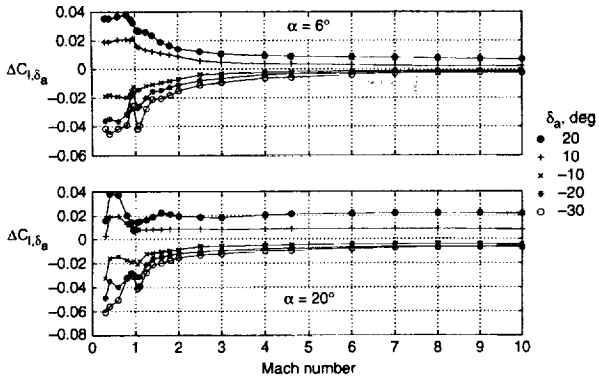

Figure 9. Aileron effectiveness at $\alpha = 6°$ and $\alpha = 20°$.

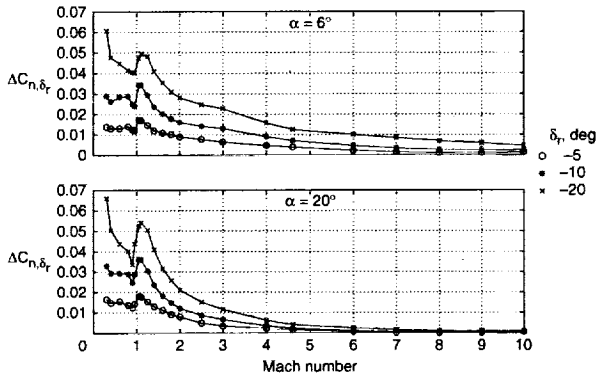

Figure 10. Rudder effectiveness at $\alpha = 6°$ and $\alpha = 20°$.

creases at transonic speeds but decreases rapidly at higher Mach numbers. At $\alpha = 20$, the rudder is virtually ineffective above Mach 5. In such situations, the X-34 flight vehicle will make use of the RCS for directional control.

The speedbrake effectiveness as measured by the drag incremental also varies in a similar fashion as shown in Figure 11. The increment in drag due to speedbrake is also accompanied by an increase in pitching moment which can augment the pitch control. The loss of rudder and speedbrake effectiveness at high angles of attack and high Mach numbers is due to the immersion of these surfaces in the low pressure wake of the fuselage and wings.

The lateral and directional stability characteristics for $\alpha = 6°$ and 18° are shown in Figures 12 and 13. It is observed that for $\alpha = 6°$, the vehicle is stable in roll ($C_{l\beta} < 0$) up to about Mach 1.7 and beyond Mach 1.7, it becomes unstable in roll ($C_{l\beta} > 0$). For $\alpha = 18°$, the vehicle is stable in roll at all Mach numbers (except around Mach1.0) due to the increasing stabilizing effect pro-

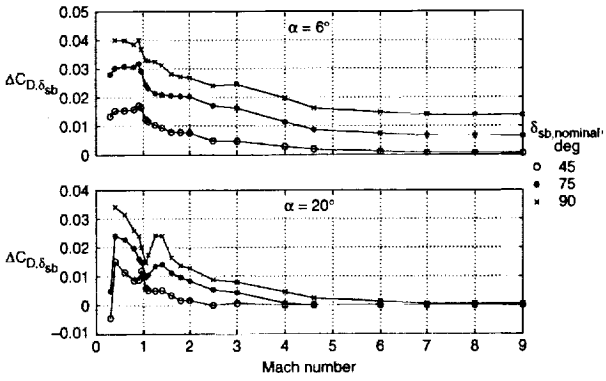

Figure 11. Speedbrake effectiveness at $\alpha = 6°$ and $\alpha = 20°$.

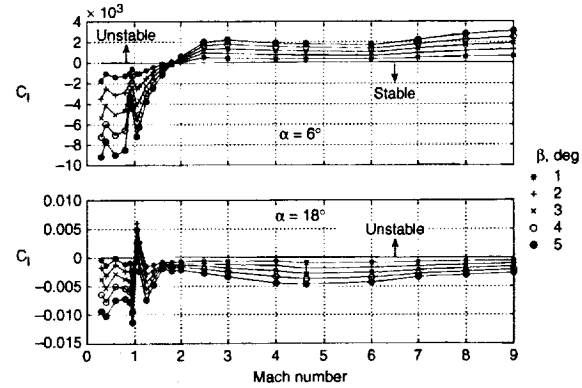

Figure 12. Rolling moment coefficient due to sideslip for the baseline configuration at $\alpha = 6°$ and $\alpha = 18°$.

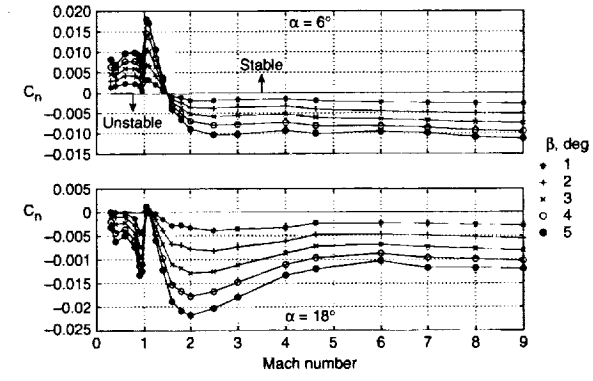

Figure 13. Variation of yawing moment coefficient for the baseline configuration at $\alpha = 6°$ and $\alpha = 18°$.

vided by the wing dihedral. For $\alpha = 6°$, the vehicle is directionally stable ($C_{n\beta} > 0$) up to Mach 1.5 and unstable ($C_{n\beta} < 0$) beyond Mach 1.5 as shown in Figure 13. For higher angles of attack ($\alpha = 18°$) the vehicle becomes directionally unstable at all Mach numbers.

The effect of landing gear deployment at low subsonic speeds (M = 0.3) is shown in Figures 14 and 15. It is observed that the landing gear deployment leads to a more nose down pitching moment up to 12° angles of attack and then the trend reverses at higher angles of attack. These incremental coefficients correspond to about half a degree of elevon deflection. Further, the vehicle experiences significant asymmetry in the variation of pitching moment coefficient with sideslip and a loss of directional stability due to landing gear deployment as observed in Figure 15. The asymmetry in the variation of pitching and yawing moment coefficients with sideslip is due to the existence of single nose gear door as discussed earlier.

The ground effect aerodynamic data for the baseline configuration are shown in Figure 16. It is observed that the incremental lift and drag coefficients are positive whereas the pitching moment increments are negative. This is to be expected because in the presence of the ground, the strength of the wing tip vortices diminishes leading to a general reduction in downwash along the wing span. In a similar fashion, the elevons and body flap were also found to be more effective in presence of the ground compared to those in free flight as shown in Figures 17 and 18.

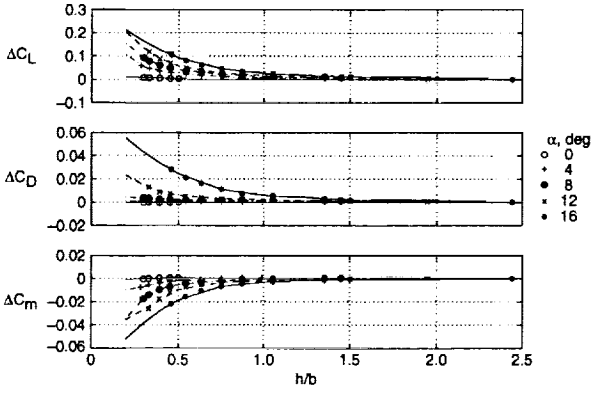

Figure 16. Incremental lift, drag and pitching moment coefficients due to baseline configuration in ground effect.

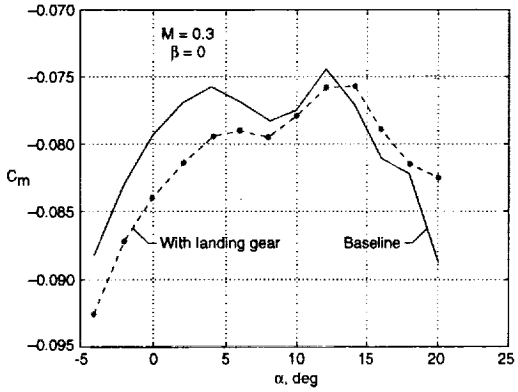

Figure 14. Effect of landing gear deployment on pitching moment coefficient

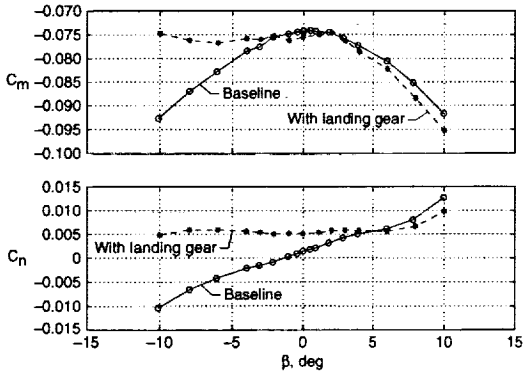

Figure 15. Combined effect of landing gear and sideslip at M = 0.3, α = 12°.

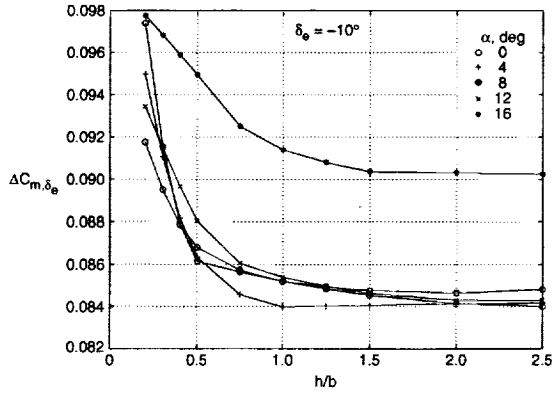

Figure 17. Elevon effectiveness in ground effect for δ_e = -10°.

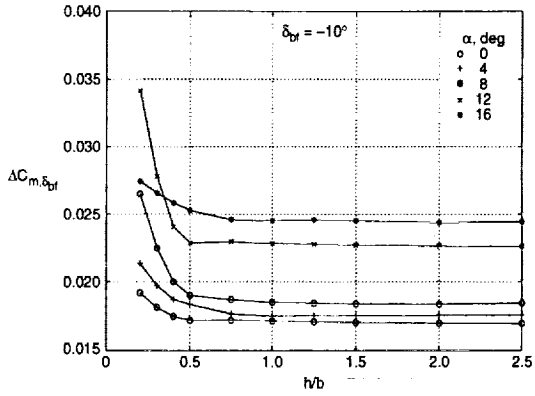

Figure 18. Body flap effectiveness in ground effect for δ_{bf} = -10°.

The ground effect test data was obtained for some combinations of angles of attack, sideslip, elevon, bodyflap and speedbrake deflections. These data were used to perform validation tests for the ground effect aerodynamic model. An example of this exercise for $\alpha = 8°$, $\beta = 4°$, $\delta_e = -10°$, $\delta_{bf} = -10°$ and $\delta_{bf} = 75°$ (nominal) is shown in Figure 19. It is observed that the lift, drag and pitching moment coefficients predicted by the ground effect aerodynamic model are within 3 or 4% of the ground effect wind tunnel test data for the combination of these parameters. However, the differences in the side force, rolling and yawing moment coefficients are much higher (Figure 19b).

The wind tunnel test Reynolds numbers for the X 34 model (based on mean aerodynamic chord) range up to 2×10^6, whereas corresponding full scale flight Reynolds numbers range up to 40×10^6. The test Reynolds numbers match the flight Reynolds numbers only for a

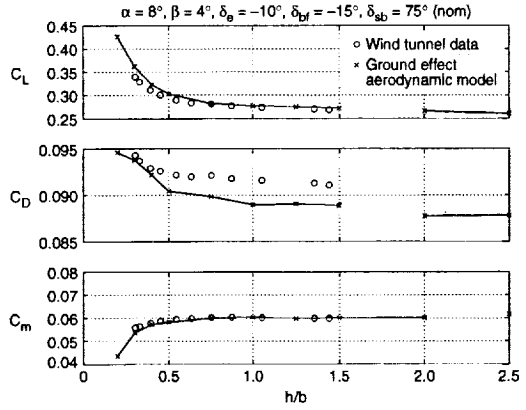

(a)

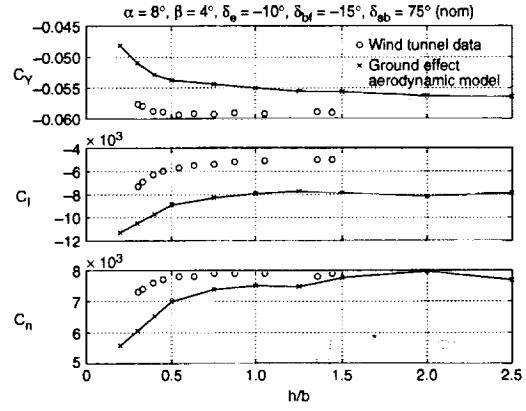

(b)

Figure 19. Validation test for ground effect aerodynamic model.

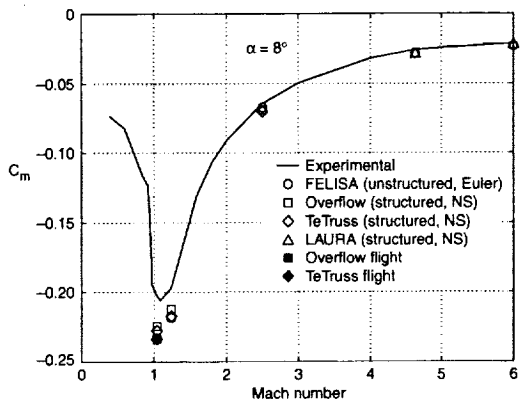

Figure 20. Pitching moment coefficient at tunnel and flight Reynolds numbers for the baseline X-34 vehicle.

segment of the hypersonic descent. Elsewhere, the flight Reynolds numbers are orders of magnitude higher than the wind tunnel test Reynolds numbers. To assess the impact of this on the pitch trim which is of critical importance during unpowered decent, LaRC has conducted a limited exercise using various computational fluid dynamics (CFD) codes. The results of this exercise are shown in Figure 20. The CFD results for the tunnel Reynolds numbers are shown by open symbols and those for the flight Reynolds numbers are shown by filled symbols. The CFD for the tunnel Reynolds numbers at Mach 1.05 and 1.25 was run with a turbulent boundary layer because the test models in the 16-Foot Transonic Tunnel were tripped. It is observed that the CFD results for Mach 2.5, 4.6 and 6.0 agree well with the wind tunnel test data. However, the CFD for Mach 1.05 and 1.25 predicts about 10% more nosedown pitching moment coefficient compared to the wind tunnel test data. Further, as shown in Figure 20, two CFD codes were run at Mach 1.05 for the flight Reynolds numbers with a turbulent boundary layer. These limited results indicate that the Reynolds number still has some influence and the flight vehicle is likely to experience a slightly higher nosedown pitching moment than predicted by the wind tunnel tests and hence the data in the aero database. This increment in nose down pitching moment approximately corresponds to about 2° of up elevon deflection. However, this aspect was not considered in applying the aerodynamic data in the database to the simulation of various flight trajectories presented in this paper.

Flight Simulation

Several X-34 Design Reference Mission (DRM) trajectories have been generated in support of the X-34 flight test program and are used for envelope expansion and flight test range planning purposes. In this paper,

four of such DRM trajectories are presented. DRM 1 refers to a typical low Mach powered flight, DRM 2 refers to the maximum burn Mach 8 flight, DRM 3 refers to a no-engine ignition abort, and DRM 4 represents a nominal unpowered approach and landing flight. DRM 1, DRM 2 and DRM 3 were generated using POST [16] and these three trajectories do not include the approach and landing phases. The DRM 4 trajectory which includes landing phase was generated using STEP [17] and makes use of the ground effect aerodynamic data in the aero database. In all these simulations, aerodynamic uncertainties including Reynolds number effects were not considered. Further, Monte Carlo simulations incorporating aerodynamic and other uncertainties are not discussed in this paper. Such simulations are currently underway in support of the flight certification program.

The DRM 1 is representative of the first powered (low Mach number) flight of the X-34 vehicle. After separation from the L-1011, the vehicle begins a pull up to engine ignition attitude. The engine is ignited and the vehicle continues a 2g pull up maneuver. The maximum dynamic pressure attained during this flight is about 600 lb/sqft. The engine burn is cutoff at a point when about 50% propellants are still remaining in the tanks. At this point, the vehicle dumps the remaining propellants and glides back to execute a standard approach and landing.

The variations of the trajectory parameters for DRM 1 are presented in Figures 21 to 24. A three dimensional plot of the flight trajectory in terms of altitude, down range and cross range is given in Figure 21. The maximum altitude reached is about 115,000 ft, the maximum Mach number reached is about 3.6 and the angle of attack goes up to about 14° during the pull up following the drop as observed in Figure 22. The time histories of the control surface deflections are shown in Figure 23. The thrust vectoring (gimbal angle) of about 15° in pitch plane is commanded initially during the ascent to augment the pitch control. The commanded elevon deflec-

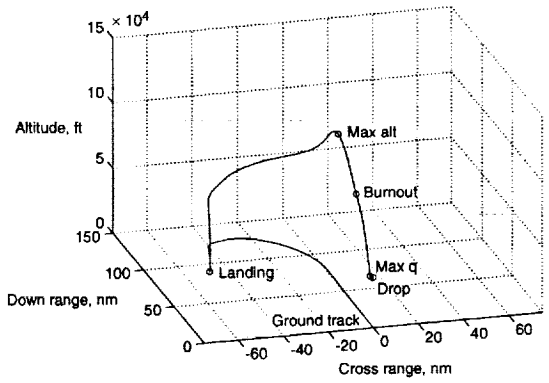

Figure 21. Variation of altitude, down range and cross range for DRM 1.

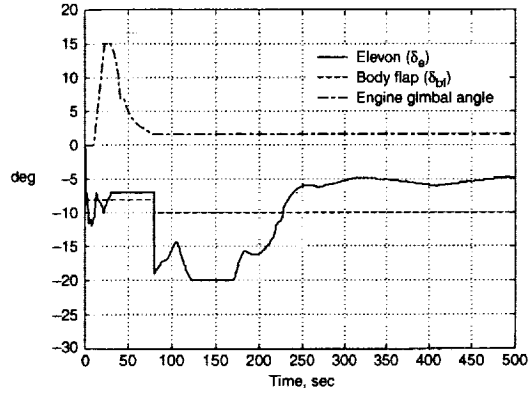

Figure 23. Time histories of control surface deflection for DRM 1.

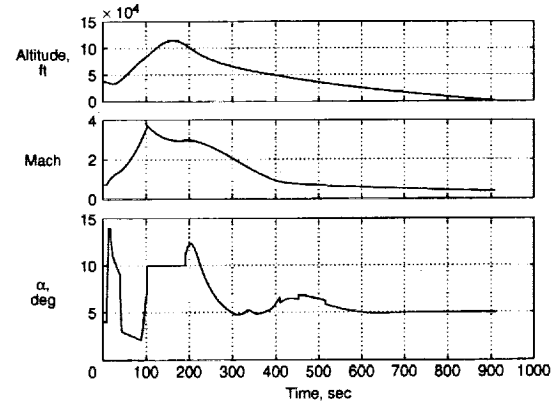

Figure 22. Time histories of altitude, Mach number and angle of attack for DRM 1.

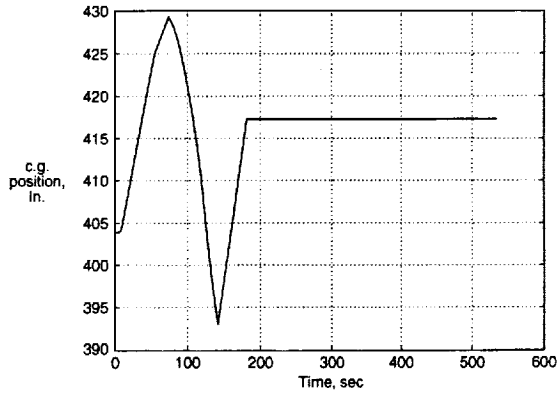

Figure 24. Variation of center of gravity during flight for DRM 1.

tions reach about –20° when the vehicle is descending around Mach 3. With the full scale vehicle likely to experience more nose down pitching moment that approximately needs an additional -2° elevon deflection to trim as discussed earlier, the actual commanded elevon deflection could be about –22°. Although these values of elevon deflection are significantly high, they are still within the permissible limits. The commanded body flap deflections go up to –7.5° during the initial part of the ascent and for the rest of the trajectory the body flap deflection remains at –10°. The center-of-gravity variation is presented in Figure 24. The center-of- gravity (c.g.) position at drop is about 404 in from the nose of the vehicle. Initially the c.g. moves aft to about 430 in and then moves forward to about 393 in and then again back to about 417 in. Subsequently, the c.g. remains at that position. This pattern of center of gravity movement is due to the manner in which LOX is consumed during the flight. The LOX is consumed first from the forward tank causing the c.g. to move aft. The subsequent forward shift followed by another rearward movement and remaining constant around 417 in is on account of sequential RP and LOX dump.

The DRM 2 is representative of a full engine burn to propellant depletion and vehicle reaching the designated altitude of 250,000 ft and target speed of Mach 8. The sequence of separation, engine ignition, and pull up are similar to the DRM 1. During this flight, the vehicle spends some time outside the atmosphere (dynamic pressure less than 1 psf) and performs an entry at 25° angle-of-attack. The RCS is used during the high altitude flight for lateral/directional control. The vehicle then follows the standard approach and landing flight path. Stagnation temperatures during entry can reach 2000°F. Envelope expansion flights will fill the gap between the low Mach DRM 1 flight and the maximum Mach 8 DRM 2 mission.

The variations of the trajectory parameters for DRM 2 are presented in Figures 25 to 28. A three dimensional plot of the altitude, down and cross ranges is given in

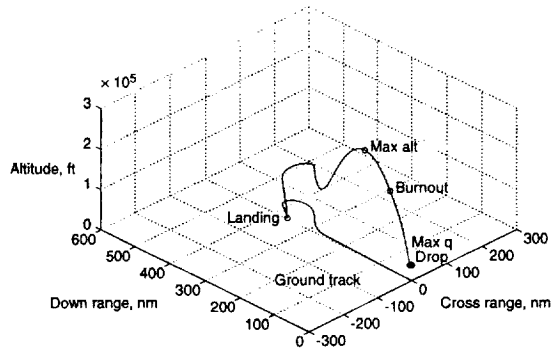

Figure 25. Variation of altitude, down range and cross range for DRM 2.

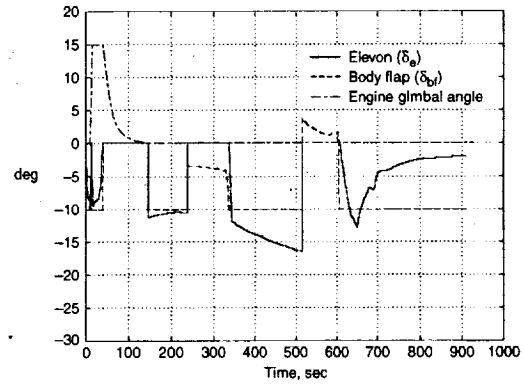

Figure 27. Time histories of control surface deflection for DRM 2.

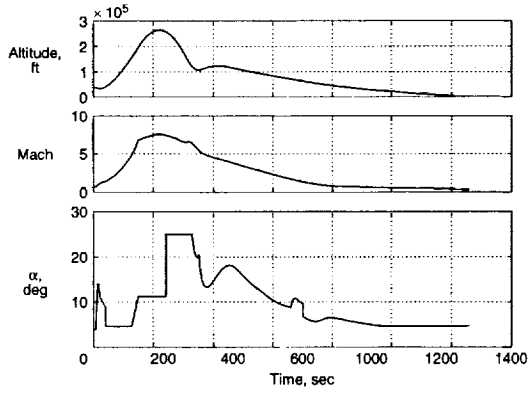

Figure 26. Time histories of altitude, Mach number and angle of attack for DRM 2.

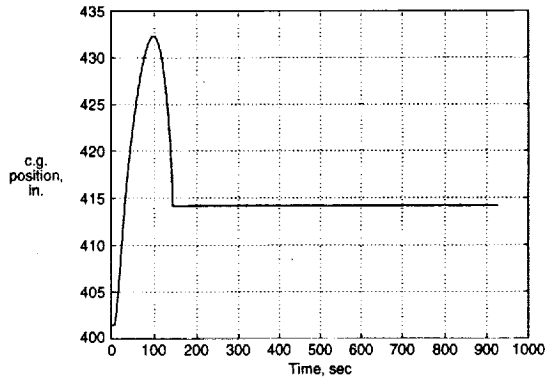

Figure 28. Variation of center of gravity during flight for DRM 2.

Figure 25. The vehicle attains its target altitude of 250,000 ft and target speed of Mach 8 around 220 seconds and then starts its unpowered descent with an angle of attack of about 25° as shown in Figure 26. The commanded elevon deflections reach about −16° while the vehicle is passing through supersonic/transonic speeds. As in DRM 1, the c.g. moves aft initially due to consumption of LOX from forward tank and then forward due to depletion of aft LOX tank. It then remains at about 414 in when all the propellants are depleted and engine burn out occurs.

The DRM 3 is an abort trajectory to deal with engine failures. Should the main engine fail to ignite after separation, a DRM 3 abort mission would be initiated in which propellants are immediately dumped and an approach and landing to the abort site is conducted. As the full propellant load is dumped, the center-of-gravity can vary greatly. The DRM 3 abort mission is not a planned flight, but would only occur in the case of engine ignition failure.

The variations of trajectory parameters for DRM 3 are shown in Figures 29 to 31. The altitude and Mach number steadily decrease following the initiation of the abort maneuver as shown in Figure 29. The commanded elevon deflections reach up to −20° towards the end as shown in Figure 30. As said before for DRM 2, even though these elevon deflections are significantly high, they are still within permissible limit. The commanded speedbrake deflections reach up to 80° at the beginning and towards the end of this mission. Note that the speedbrake deflections were not commanded during DRM 1 and DRM 2. The variation of the c.g. is shown in Figure 31. The initial aft movement followed by the forward movement and then remaining constant around 420 in are all caused by the sequential dumping of the RP and LOX.

The unpowered approach and landing test (DRM 4) will constitute the first unpowered flight of the X-34 vehicle. After release from the L-1011, the unfueled X-34 acquires the approach flight path and conducts a standard approach and landing. The variation of the trajectory parameters for DRM 4 are shown in Figures 32 and 33. It is observed that the vehicle lands around an angle of attack of 8°. The commanded elevon, body flap and speedbrake deflections are within limits as in DRM 1 to DRM 3.

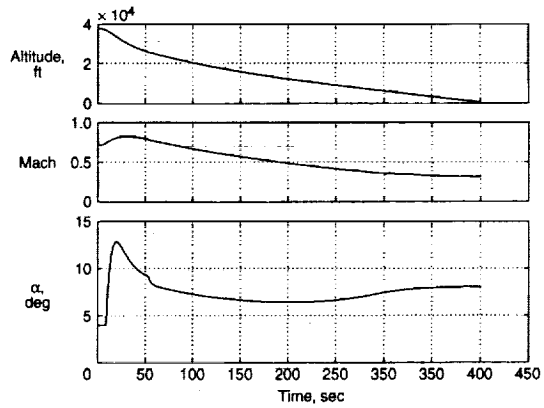

Figure 29. Time histories of altitude, Mach number and angle of attack for DRM 3.

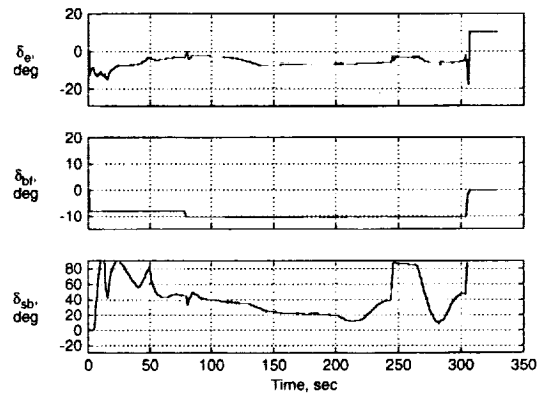

Figure 30. Time histories of control surface deflection for DRM 3.

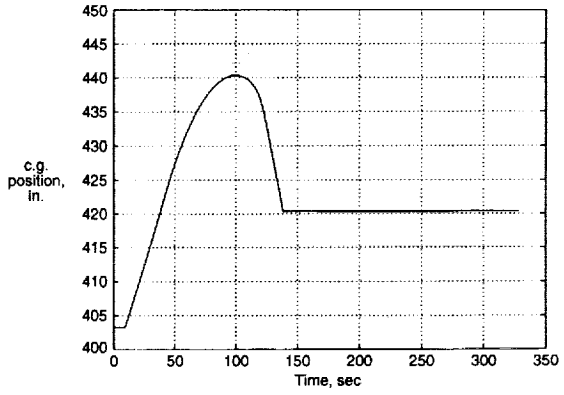

Figure 31. Variation of center of gravity during flight for DRM 3.

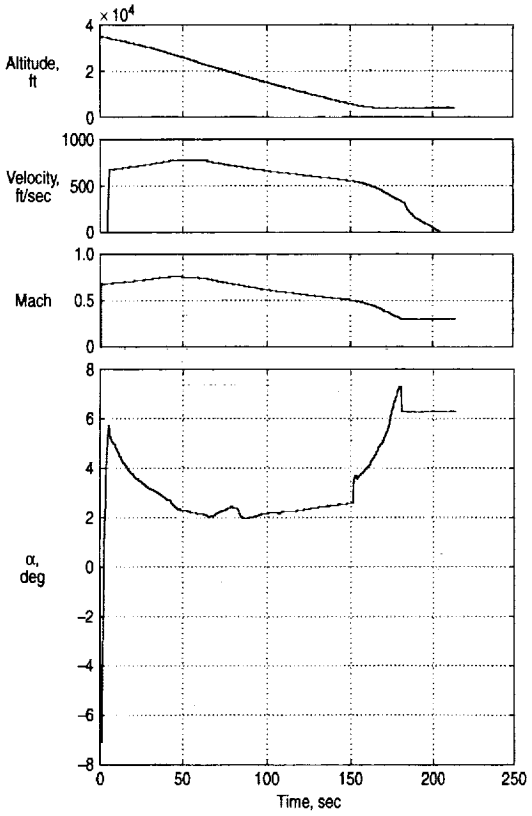

Figure 32. Time histories of altitude, velocity, Mach number and angle of attack for DRM 4.

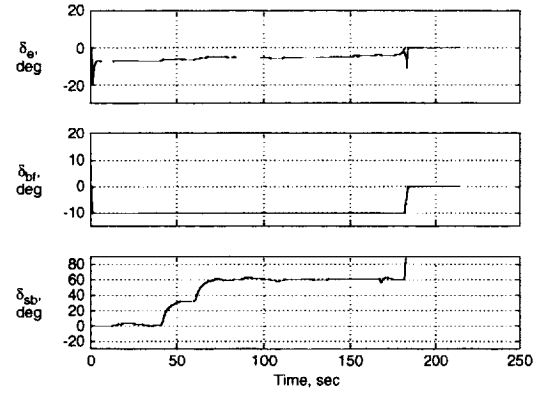

Figure 33. Time histories of control surface deflection for DRM 4.

CONCLUDING REMARKS

This paper has presented an overview of the aerodynamic characteristics, the development of the preflight aerodynamic database and flight simulations of the NASA/Orbital X-34 vehicle. The aerodynamic data in the database is provided for both free flight and flight in ground effect and covers the complete range of Mach numbers, angles of attack, sideslip and control surface deflections expected in the entire flight envelope of the X-34 vehicle. The variations of the trajectory parameters and control time histories for four design reference missions which are representative of the X-34 flight test program indicate that the vehicle performs these missions satisfactorily and the commanded control deflections are within the permissible limits at all points along these flight trajectories.

ACKNOWLEDGEMENT

Authors are thankful to Jim Weilmuenster, Ken Sutton, Peter Buning, Ram Prabhu and Shahyar Pirzadeh of NASA Langley for the CFD calculations.

REFERENCES

1) Freeman, D.C. Jr., Talay, T.A., and Austin R.E.: *Reusable Launch Vehicle Technology Program*, IAF 96-V.4.01, October 1996.

2) NASA: *Reusable Launch Vehicle (RLV), Small Reusable Booster, X-34*, Cooperative Agreement Notice, CAN 8-2, January 1995.

3) Brauchmann, G.J.; *X-34 Vehicle Aerodynamic Characteristics*, Journal of Spacecraft and Rockets, Vol. 36, No. 2, 1999, pp. 229-239.

4) Pamadi, B.N., and Brauchmann, G.J.; *Aerodynamic Characteristics and Development of the Aerodynamic Database of the X-34 Reusable Launch Vehicle*, Paper No. 17.1, International Symposium on Atmospheric Reentry Vehicles and Systems, March 16-18, 1999, Arcachon, France.

5) Wurster, K. E., Riley C.J., and Vincent Zoby E.; *Engineering Aerothermal Analysis for X-34 Thermal Protection System Design*, AIAA Paper 98-0882, January 1998.

6) Gentry, C. E., Quinto, P.F., Gatlin, G.M., Gregory, M., and Applin, Z.T.: *The Langley 14- by 22- Foot Subsonic Tunnel: Description, Flow Characteristics and Guide for Users*, NASA TP-3008, September 1990.

7) Capone, F.J., Bangert, L.S., Asbury, S.C., Mills, C.T., and Bare, E.A.: *The NASA Langley 16- Foot Transonic Tunnel*, NASA TP-3521, September 1995.

8) Jackson, C.M., Corlett, W.A., and Monta, W.J.: *Description and Calibration of the Langley Unitary Plan Wind Tunnel*, NASA TP-1905, November 1981.

9) Micol, J.M.: *Hypersonic Aerodynamic/Aerothermodynamic Testing Capabilities at Langley Research Center: Aerodynamic Facilities Complex,* AIAA Paper 95-2107, 1995.

10) Rockwell International Space Division.: *Aerodynamic Design Data Book, Vol. I, Orbiter Vehicle*, Report No. SD 72-SH-0060-1L, November 1977.

11) Bonner, E., Clever, W., and Dunn, K.: *Aerodynamic Preliminary Analysis System II, Part I- Theory*, NASA CR-165627, 1989.

12) Divan, P., and Sova, G.: *Aerodynamic Preliminary Analysis System II, Part II- User's Manual*, NASA CR-165628, 1989.

13) Cruz, C., and Wilhite, A.: *Prediction of High-Speed Aerodynamic Characteristics Using Aerodynamic Preliminary Analysis System (APAS),* AIAA Paper No. 89-2173, 1989.

14) Cruz, C., and Ware, G.: *Predicted Aerodynamic Characteristics for HL-20 Lifting Body Using the Aerodynamic Preliminary Analysis System (APAS),* AIAA Paper No. 92-3941, 1992.

15) Cruz, C., and Engelund, W.C.: *An Aerodynamic Preliminary Analysis System (APAS) Calibration Report: Space Shuttle Orbiter*, Paper presented at the Society of Hispanic Professional Engineers 6th Annual Eastern Technical and Career Conference, Washington D.C., November 12-14, 1992.

16) Brauer, G. L., Cornick, D. E., and Stevenson, R.; *Capabilities and Applications of the Program to Optimize Simulated Trajectories (POST)*, NASA CR-2770, February 1977.

17) STEP: *PEGASUS NASA Six Degree of Freedom (6DOF) Simulation User's Manual*, Orbital TM–11787, 30 June 1995.